PAPER

Check for updates

Polymerization mechanism of 4-APN and a new catalyst for phthalonitrile resin polymerization

Liping Sheng, [ID] *[a] Kerui Xiang,[a] Rong Qiu,[a] Yuxuan Wang,[a] Shengpei Su,[a] Dulin Yin[a] and Yongming Chen [ID] *[b]

The widely used catalysts for phthalonitrile (PN) resin polymerization are aromatic compounds containing $-NH_2$ because of their high catalytic performances. However, the catalytic mechanisms of these catalysts are not very clear. To understand the mechanisms of them, the widely used autocatalytic catalyst 4-(4-aminophenoxy)-phthalonitrile (4-APN) was studied in this paper. The polymerization process of 4-APN was tracked by a multi-purpose method, and ammonia gas was detected during the cross-linking processing for the fist time. Combined with the online IR results of the curing process of 4-APN, the mechanism of ammonia generation was newly proposed. Based on this mechanism, a new catalyst selection strategy was promoted, which is different from the traditional approach to catalyst selection for PN resin polymerization. According to the new strategy, 1,3-diiminoisoindoline (1,3-DII) was selected as a novel catalyst. The results showed that the new catalyst could not only effectively catalyze the polymerization of PN resin, but also has a lower curing temperature than that of organic amine catalysts and can eliminate the release of ammonia gas and the voids in the products caused thereby. Therefore, the results of this study will give important enlightenment to the development of PN catalysts and the development of PN.

1 Introduction

Phthalonitrile (PN) resin, as a representative high-performance resin, has many excellent properties, such as excellent mechanical properties, heat resistance, moisture resistance, corrosion resistance, ablation resistance, and so on.[1–5] However, the early application of phthalonitrile was hindered by its extremely difficult polymerization and reaction inertness.[6–8] Subsequently, researchers found that different catalysts, including amines, phenols, carboxylic acids, and inorganic salts, could drastically reduce the curing temperature and reduce the curing time.[7–9] This promoted the development of PN resin,[9,11] which has happened rapidly over the past 20 years.[12–18]

Among these PN catalysts, the catalysts containing $-NH_2$ have the highest outstanding catalytic performance and have been widely used,[19–24] such as *p*-BAPS,[25] *m*-APB,[26] 4-APN,[5] *etc.* (shown in Fig. 1). Although the catalytic performance of the compounds containing $-NH_2$ has been well recognized, the polymerization crosslinking mechanisms are not clearly understood. At present, the presence of void defects is a common phenomenon for the PN polymer products cured with the catalysts containing $-NH_2$. These

void defects can seriously weak the mechanical properties. Evidences indicated that this shortage was mainly caused by lower thermal stability of the catalysts.[27,28] The later reported 4-APN catalyst could solve the problem by catalyzing –CN polymerization through participating in the CN polymerization.[29] However, the mechanical properties of these polymers cured by 4-APN are still unsatisfied.[30]

To fully understand and solve of this problem, in this paper, the polymerization process of 4-APN was traced by an integrated multi-techniques method. The small molecules released during the polymerization of 4-APN was monitored and analyzed by thermogravimetric infrared (TG-IR). Combining with the online infrared information of the curing process of 4-APN, the polymerization mechanism of 4-APN was proposed. According to the proposed mechanism in this article, a new catalyst selection strategy was promoted and 1,3-diiminoisoindoline (1,3-DII) was selected and used as a new PN catalyst. Then, a series of good results appeared. For example, the 1,3-DII had the lowest reported cure temperature as the organic PN catalyst. And the PN
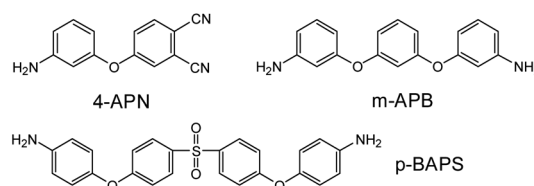
[a]National Local Joint Engineering Laboratory for New Petro-chemical Materials and Fine Utilization of Resources, College of Chemistry and Chemical Engineering, Hunan Normal University, Changsha, 410081, P. R. China. E-mail: sleeping1217@126.com

[b]Center for Functional Biomaterials, School of Materials Science and Engineering, Key Laboratory for Polymeric Composite and Functional Materials of Ministry of Education, Sun Yat-sen University, Guangzhou 510275, China

Fig. 1 The chemical structure of 4-APN, *m*-APB, *p*-BAPS.

polymer cured by 1,3-DII was difficult to be found voids defects through SEM. Therefore, we believe that our study will give important inspirations for the development and design of new PN catalysts and new PN monomers.

2 Experiments

2.1 Materials

4-Nitrophthalonitrile (AR, 99%) was purchased from Shijiazhuang Aifa Chemical Technology Co., Ltd (Hebei, China) and used as received. *P*-Aminophenol (AR, 99%) was commercially available from Sinopharm Chemical Reagent Co., Ltd (Shanghai, China) and used as received. Chromatographic purity *N,N*-dimethylformamide (DMF, HPLC, 99.8%), was purchased from Tianjin Kemiou Chemical Reagent Co., Ltd and dehydrated for 3 days by 4 Å molecular sieves before using. Anhydrous potassium carbonate (AR, 99%) and sodium hydroxide (AR, 99%) were used as received from Beijing Beihua Fine Chemicals Co., China. Phenol (AR, 99%), hydroquinone (AR, 99%) and concentrated hydrochloric acid (AR, 36–38%) were all from Chengdu Kelon Chemical Reagent Factory and used as received. Resorcinol (AR, 99%) was from Xiangzhong Fine Chemicals Factory and used as received.

2.2 Synthesis

2.2.1 The synthesis of 4-(4-aminophenoxy)-phthalonitrile (4-APN). 4-APN was synthesized according to the ref. 10 and 11. Yield: 80%. Purity (HPLC): >99%. Melting point (mp, DSC): 134.5 °C. Its chemical structure was characterized and identified by ^{1}H NMR (400 MHz, CDCl$_3$, δ, ppm): 7.67 (dd, $J_1 = 8.5$ Hz, $J_2 = 3.8$ Hz, 1H), 7.25 (d, $J = 4.0$ Hz, 1H), 7.18 (d, $J = 2.4$ Hz, 1H), 6.91–6.79 (m, 2H), 6.78–6.67 (m, 2H), 3.73 (s, 2H).

2.2.2 The synthesis of arylene ether phthalonitrile (PEN). Resorcinol (6 mmol), anhydrous potassium carbonate (0.012 mmol), *N*-methylpyrrolidone (NMP, 20 ml), and toluene (20 ml) were added in a three-neck round bottom flask equipped with a mechanical stirring, a water separator and a reflux condenser. The system was purged with a flow of nitrogen. The mixture was stirred and refluxed at 140 °C, until the water volume collected in the water separator no longer increases. Then, the reaction temperature was raised to 170 °C, and the residual toluene was distilled out. After removing all toluene, the reaction mixture was stirred and cooled down to room temperature. 2,6-Dichlorobenzonitrile (0.003 mol) was then added, and the mixture kept refluxing at 200 °C for 5 hours. Then cooled down to room temperature, 4-nitrophthalonitrile (0.006 mol) was added and the mixture was stirred at 80 °C for 8 hours. The final mixture was poured into ethanol, suction-filtered, and washed repeatedly with pure water, vacuum dried the resulting solid, and then passed through a silica gel column. The eluent was petroleum ether and ethyl acetate. The volume ratio is 1 : 0.5. Finally the target was obtained after evaporation and vacuum drying.

^{1}H NMR (400 MHz, DMSO, δ, ppm): 8.09 (d, $J = 8.7$ Hz, 2H), 7.87 (d, $J = 2.6$ Hz, 2H), 7.60–7.52 (m, 4H), 7.48 (dd, $J = 8.8$, 2.6 Hz, 2H), 7.12 (t, $J = 2.0$ Hz, 2H), 7.11–7.08 (m, 2H), 7.08–7.05 (m, 1H), 6.81 (d, $J = 8.5$ Hz, 2H). The mass spectrometric result shows that the molecular peak was 570, and the theoretical molecular weight was 571, which indicating that the obtained was the target.

2.3 Preparation of PN mixtures and their curing procedures

The catalyst (4-APN or 1,3-DII) and PEN were weighted accurately. The mass ratio of catalyst to PN is of 25 to 100. Then mixing and grinding them well, a milligram-level amount of the mixture was taken for DSC testing. As the heating rate increasing, the exothermic peak of DSC drifts toward the high temperature. Therefore, the isothermal curing of the two mixtures was performed at 166 °C and 249 °C respectively, and the curing time of the two mixtures were 4 h.

2.4 Characterization

1H-NMR spectra was collected using an Agilent DD2 400-MR spectrometer, operating at 400 MHz using DMSO and CDCl$_3$ as solvents. TGA-IR-GC-MS test was conducted using the PerkinElmer Thermogravimetric Analyzer Pyris 1 TGA, the PerkinElmer FT-IR/FIR Frontier, the PerkinElmer Gas Chromatograph Clarus 680, and the PerkinElmer Mass Spectrometer Clarus SQ8T. The TGA condition was that the heating rate was 20 °C min^{-1} under helium atmosphere with a flowing rate of 30 ml min^{-1} from 50 °C to 550 °C. The IR sample cell temperature was 300 °C, scanning from 400 cm^{-1} to 4000 cm^{-1}. The temperature of the tube between TGA and IR was 300 °C or 50 °C. The conditions of GC were as follow: inject port temperature was 300 °C, oven program was 20 °C min^{-1} from 80 °C to 320 °C, Elite-5MS column. And the condition of MS was EI ionization, the energy of ionization was 70 eV, the ionization temperature was 275 °C. DSC curves were collected through Mettler-Toledo (DSC1 STAR System) at a heating rate of 10 °C min^{-1} from 50 °C to 400 °C, flowing at 40 ml min^{-1} of high purity N$_2$. TGA curves were collected through Mettler-Toledo (TGA/DSC1 STAR System) at a heating rate of 10 °C min^{-1} from 50 °C to 400 °C or from 50 °C to 800 °C, flowing at 100 ml min^{-1} of high purity N$_2$. The online FTIR spectra were collected by combing the heating controller of HAKKE Rheometer instrument MARS III and FTIR instrument of PerkinElmer FT-IR/FIR Frontier. The samples (0.3–0.5 g) were melted on the IR sample stage of Rheometer instrument with a heating rate of 2 °C min^{-1} from melting point to 350 °C. A synchronous IR collection was realized by FTIR instrument of PerkinElmer FT-IR/FIR Frontier. The morphology of cured polymers from PN mixtures were observed by scanning electron microscope (SEM), Hitachi S4800 Japan.

3 Results and discussion

3.1 The reactivity and thermal stability of 4-APN

The chemical structure of 4-APN is shown in Fig. 1. The DSC, TGA and DTG curves of it from 25 °C to 400 °C are shown in Fig. 2(a). It shows that the total weight loss is 12% from 25 °C to 400 °C. It is about 11% weight loss around 314 °C. And it is at this temperature that the DTG and DSC peaks overlap. The degradation temperature and the char yield at 800 °C of the
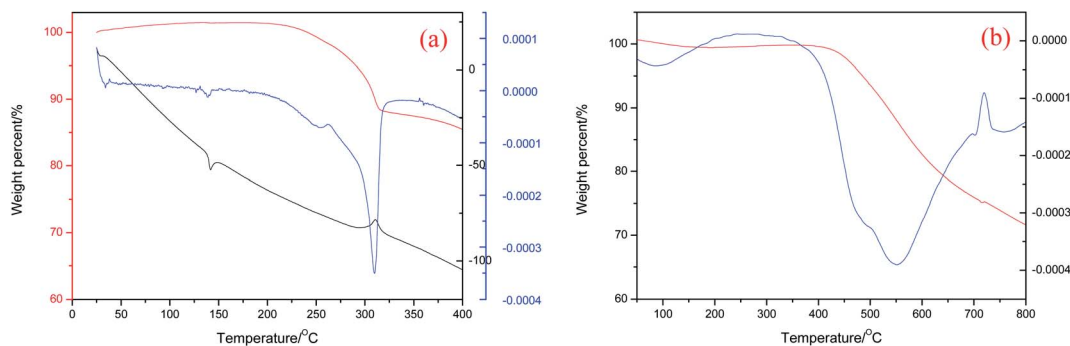
Fig. 2 TGA, DSC, and DTG curves of 4-APN (a) and the TGA and DTG curves of the cured polymer from 4-APN (b).

polymer cured from 4-APN are 550 °C and 71.6% respectively (Fig. 2(b)). These results indicate that the weight loss and the curing reaction almost occur at the same time and the derived polymer has an excellent thermal stability. However, it is generally believed that the reaction between nitriles is additive polymerization, and no small molecules are released, so there should be no weight loss. Therefore, we assumed that there might be some small molecules were released in the reaction between amine and nitrile, which leaded to the weight loss.

3.2 The polymerization process of 4-APN

Then, the polymerization process of 4-APN was monitored through TG-IR-GC-MS. In this experiment, the thermogravimeter was used to control the cure temperature accurately. The small molecules generated during the polymerization are carried into the IR gas sample chamber along with the protective gas flow. The GC then collects the mixed gas from IR sample chamber and injects it into the GC instrument. Finally, the separated ingredients from the GC are detected by MS. Fig. 3 is the TGA curve from the TG-IR-GC-MS method. It shows that there is a serious weight loss in the range of 300 °C to 400 °C. At 400 °C, the total loss weight is 35%, which is far higher than that of from the singer technique of TGA. This may be caused by two reasons: first, the high vacuum of the interior of the combined instrument reduces the boiling point of 4-APN, leading to the increase evaporation of 4-APN. Second, small

molecules may be produced during the cross-linking reaction, which aggravates the weightlessness. Therefore, adjusting the temperature of the connecting tube between the TG and IR, the infrared spectra of the compounds with different boiling points can be collected.

When the temperature of the connecting tube between the TG and IR was set as 300 °C, Fig. 4 was collected. In Fig. 4, it shows clearly that the characteristic peaks of CN (2237 cm^{-1}) and $-NH_2$(3370 cm^{-1}, 3455 cm^{-1}), and the concentration of them does not decrease for a long period of time (618 s − 529 s = 89 s). The 529 seconds infrared spectrum was extracted and compared with the IR spectrum of 4-APN, and it was found that their two spectra were completely coincident (Fig. 5). This proves that 4-APN does have a large amount of volatilization under such a high vacuum environment.

Then, the connecting tube temperature was set as 50 °C, and Fig. 6 was collected. It was found that new compounds appearance in the 937 s, which was later than the evaporation of 4-APN (529–618 s). Its appearance temperature is about 362 °C, which is much higher than the initial evaporation temperature (226 °C) and curing temperature (314 °C) of 4-APN. However, the boiling point of this substance is less than 50 °C. This indicates that the low boiling point compound in Fig. 2 may come from the cross-linking reaction. In addition, the Abs value of the compound in Fig. 2 is not only much lower than that of 4-APN, but also gradually decreases over time. This indicates that the
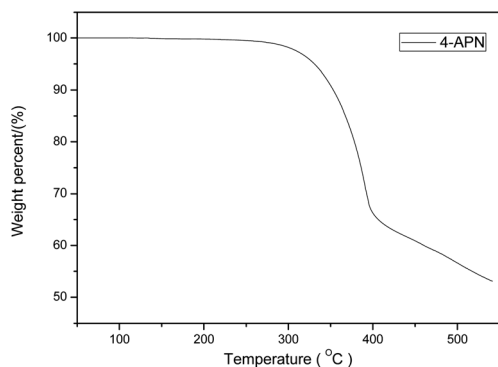

Fig. 3 The TGA curve of 4-APN from TG-IR-GC-MS at a heating rate of 20 °C min^{-1}.
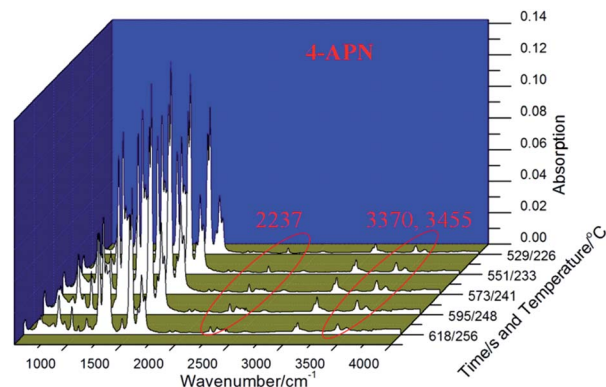

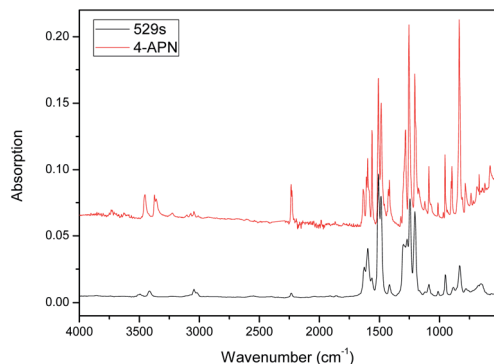**Fig. 4** IR waterfall plot when connection tube temperature is 300 °C.

Fig. 5 The IR spectra of the 4-APN and the 529 s from TG-IR-GC-MS.
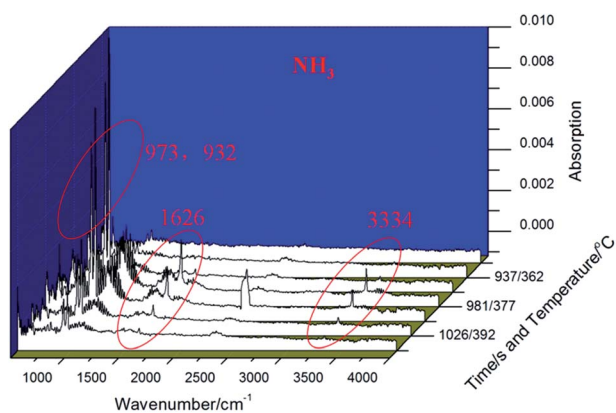

Fig. 6 IR waterfall plot when connection tube temperature is 50 °C.

compound is a trace substance and gradually disappears as the reaction is over. The infrared spectrum of 959 seconds in Fig. 6 was extracted as Fig. 7(a). Fig. 7(a) shows that 3334 cm^{-1} is the stretching vibration of N–H, 1626 cm^{-1} is the out-of-plane bending vibration of N–H, and 973 cm^{-1} and 923 cm^{-1} are the bending vibration of N–H. Compared with the standard spectrum of ammonia (Fig. 7(b)), their similarity is over 95%. Therefore, we conclude that the compounds in Fig. 6 and 7(a) are ammonia gas.

The ammonia gas produced by the cross-linking reaction was collected, mixed with the protective gas flow, and then injected into the GC-MS sample tube together. The mixture was separated by a GC column, and then detected by an MS instrument. The chromatogram and mass spectra of the
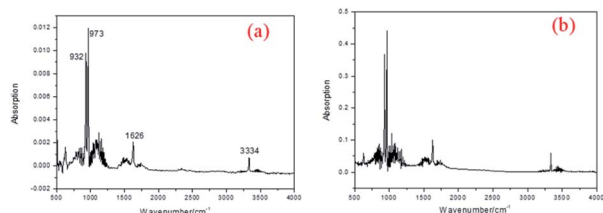

Fig. 7 The IR spectrum when connecting pipe temperature is 50 °C (a) and standard IR spectrum of NH$_3$ (b).

mixture were collected and shown in Fig. 8(a) and (b). In Fig. 8(a), there is only one peak in the mixture chromatogram curve, which means that the released small molecular and carrier gas had not been separated. This result may be due to the extremely small amount of ammonia produced by the cross-linking reaction, causing the GC column to be unable to separate it from the carrier gas. To identify the released substances again, we compared the mass spectra of the carrier gas and the mixture in detail. In Fig. 8(b), there are three more MS peaks of the mixture, 34, 15, and 2, when comparing with that of the carrier gas. Based on the fragment ion peaks, the possible cleavage pathway is brought forward, as shown in Fig. 8(c). These results show that these three peaks are completely consistent with the ammonia ion cleavage process. Therefore, based on the GC-MS result, it can be confirmed again that the released compound is ammonia.

3.3 The possible polymerization mechanism of 4-APN

From the above analysis, we realize that ammonia is produced by 4-APN polymerization reaction. But what is the mechanism of ammonia production? What other products are formed? To find answers to these questions, the curing process of 4-APN was tracked by online infrared technology. Fig. 9 shows the changes in infrared spectra during the curing process of 4-APN.

In Fig. 9(a), as the temperature increases, the CN (2227 cm^{-1}) group begins to crosslink and its content gradually decreases. However, its content has not been decrease to zero. This indicates that a large number of CN groups participate in the crosslinking reaction, but not all of them, and there are still some residues. The primary amino groups, corresponding to 3469 cm^{-1} and 3378 cm^{-1}, decrease simultaneously with CN. This indicates that –NH$_2$ may participate in the crosslinking reaction of CN. At the same time, the IR peaks of imine group (–NH–) at 3421 cm^{-1} increased slightly, indicating that the –NH$_2$ involved in the CN crosslinking reaction may be converted into –NH– group. Meanwhile, the shoulder peak at 3000–3059 cm^{-1} increased slightly, indicating that the content of unsaturated = C–H bond increased, which may be due to the formation of new unsaturated rings. In Fig. 9(b), many new absorption peaks appear in the range of 500–1750 cm^{-1}. For example, between 1650–1400 cm^{-1}, this region is basically considered to be a stretching vibration of various ring-conjugated double bonds. Therefore, the stretching vibrations of the benzene ring and the heterocyclic ring overlap here and cannot be distinguished. The strong changes at 1650/1602/1558/1502/1486 cm^{-1} all indicate that some new conjugate rings are generated. The 1400–1000 cm^{-1} is mainly the stretching vibration of the single bond connected to different rings, such as new peaks at 1350 cm^{-1} and 1035 cm^{-1}, corresponding to Ar–O and Ar–N respectively. In addition, the bending vibration at 500–600 cm^{-1} is significantly weakened, which may be closely related to the conversion of –X–H to ring =X–H.

At present, researchers basically believe that CN polymerization mainly produces triazine, isoindole and phthalocyanine rings,[31–42] does not produce small molecules, and gives the
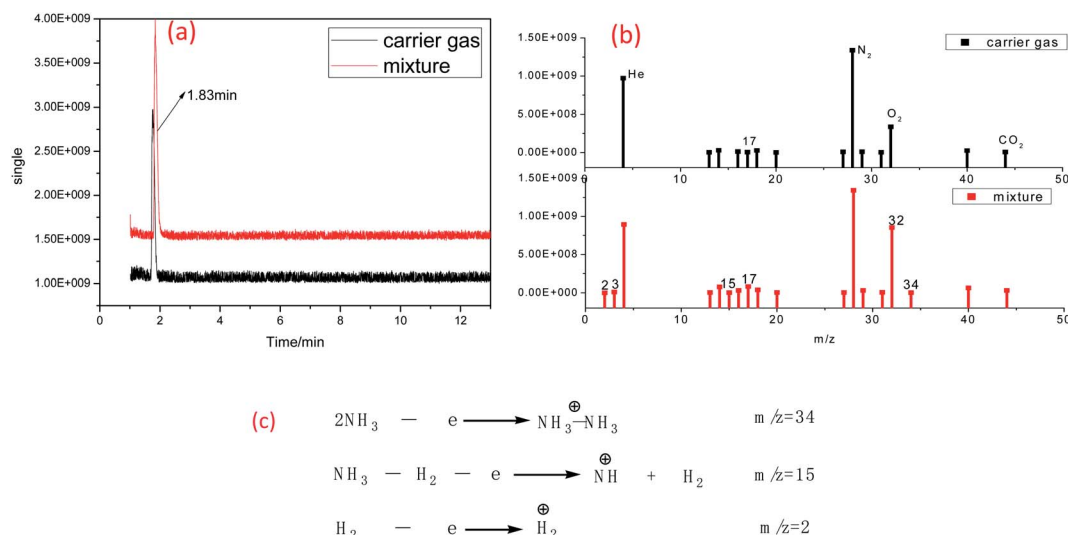
Fig. 8 The gas chromatography ((a), the red is mixture gas, the black is carrier gas), the mass spectrogram when retention time is 1.83 min on GC ((b), the red for mixture gas, the black for carrier gas), the split process of the three more peaks in the MS spectra of the mixture gas (c).
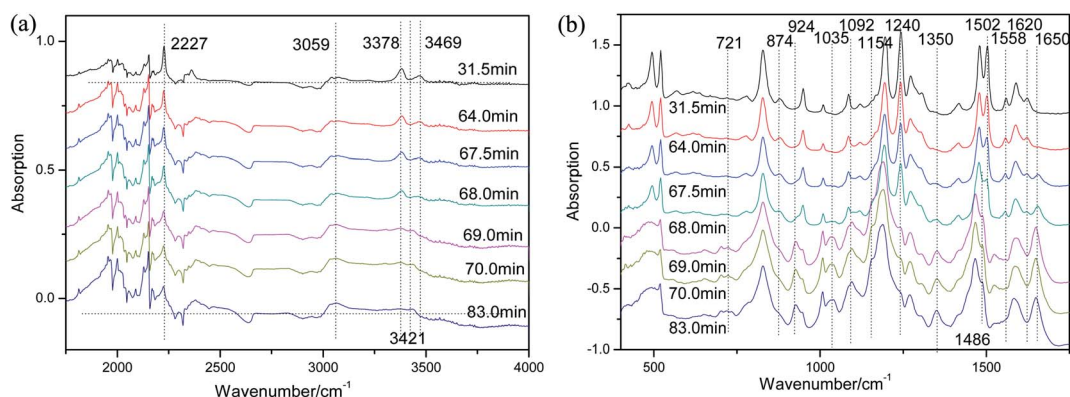

Fig. 9 The online IR spectra during the curing of 4-APN ((a) wavenumber is 400–1750 cm^{-1}; (b) wavenumber is 1750–4000 cm^{-1}, the heating rate is 2 °C min^{-1}).

polymerization mechanism of forming the three heterocycles. However, this does not explain the experimental results in this paper very well. Therefore, combined with the experimental results in this paper, we give the following polymerization mechanism (Fig. 10).

The specific mechanism is as follows. First, the active proton on –NH$_2$ attacks the unsaturated CN, the triple bond opens, the proton are transferred to the negative N of CN, and the electron-rich N in –NH$_2$ is connected to the electron-deficient C of CN, generating –NH–C(Ar)=NH. The proton in =NH further attacks the adjacent CN on the same benzene ring, forming a relatively stable five-membered ring, isoindole, while producing another unsaturated imine group =NH, as shown in Fig. 10(A–B). The second =NH can continue to catalyze CN on another 4-APN, forming another isoindole ring and unsaturated =NH, as shown in Fig. 10(B–E–H). Alternatively, the proton on the second unsaturated =NH can also be transferred to the primary amine group –NH$_2$ of 4-APN, releasing ammonia and

forming a more stable conjugated polycyclic ring, as shown in Fig. 10(B–C–F). Alternatively, the H of –NH on B can be transferred to the –NH$_2$ of 4-APN, forming an ammonia and a tertiary amine center, as shown in Fig. 10(B–D–G). Of course, the B–G route has a much lower probability than the B–F route, due to steric hindrance.

It can be seen from the above mechanism that at least three 4-APN molecules can release one ammonia. Therefore, theoretically, the maximum amount of ammonia ($w\%$) released during the 4-APN polymerization process can reach 2.41%. The specific calculation process is as follows:

$$w\% = \frac{M_{NH_3}}{3M_{4\text{-}APN}} \times 100\%$$

In the above formula, M_{NH_3} is for the molar molecular weight of ammonia, $M_{4\text{-}APN}$ is for the molar molecular weight of 4-APN, and $w\%$ is for the maximum mass percentage of ammonia gas produced. However, it can be seen from the thermogravimetric diagram that the actual total weight loss is much greater than
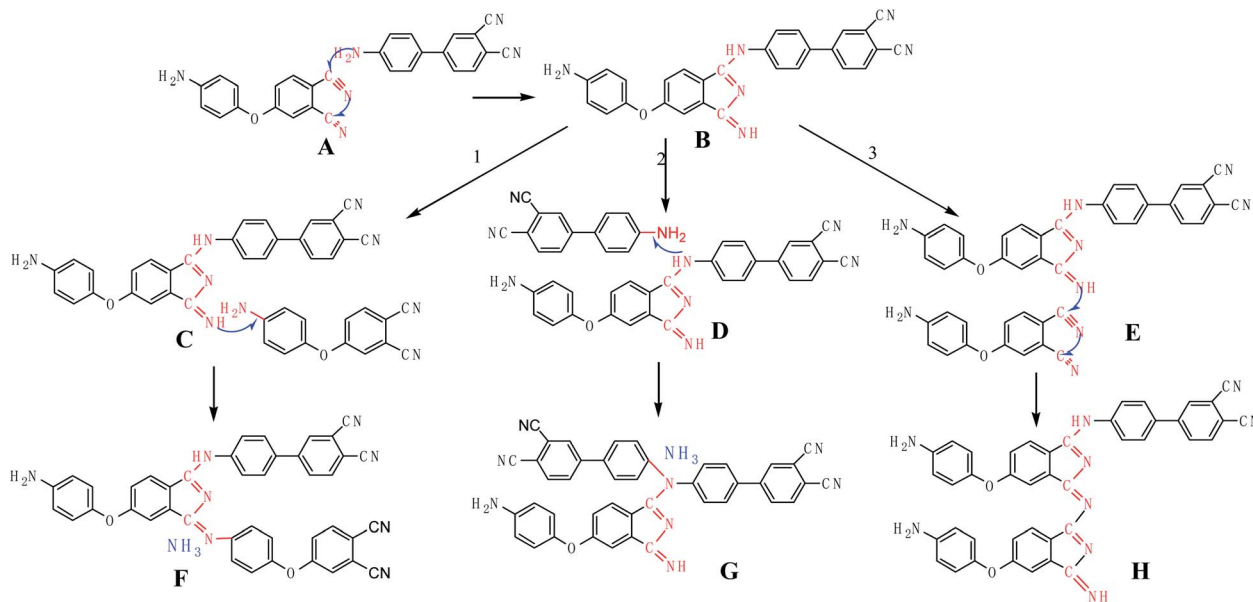
Fig. 10 The possible cure reactions of 4-APN.

2.41%. This extra part may come from the evaporation of 4-APN. During the cross-linking process, a large amount of reaction heat is released rapidly, which aggravates 4-APN boiling and further aggravates the weight loss percentage.

The above mechanism also shows that both primary amino groups and unsaturated =NH can catalyze CN polymerization. However, when the primary amino group encounters unsaturation =NH, ammonia will be released. When –NH$_2$ catalyzes the CN polymerization, it will produce =NH, so –NH$_2$ catalyzes CN polymerization will produce ammonia. Ammonia will form pores in the cured polymer, seriously damaging the mechanical properties of the cured product. Therefore, unsaturated =NH may be more suitable for catalyzing CN polymerization than primary amino groups.

3.4 The novel catalyst for PN resin

According to the polymerization mechanism of 4-APN proposed in this article, the following compound 1,3-diiminoisoindoline (1,3-DII, see Fig. 11(a)) was selected and used as a new catalyst

for PN resin. In Fig. 11(a), the melting point temperature of 1,3-DII is 175 °C, and the exothermic peak of the PN mixture containing 1,3-DII appears at 176 °C. In Fig. 11(b), the melting point temperature of 4-APN is 134 °C, and the exothermic peak of the mixture containing 4-APN is 259 °C. All these indicates that the new catalyst 1,3-DII not only can catalyze the polymerization of the PN resin, but also the curing temperature of 1,3-DII is much lower than that of 4-APN. It also shows that the exothermic peak shape of the PN mixture with 1,3-DII is much gentle than that of with 4-APN. This is more conducive to high-precision preparation of thick-wall composites.

Then, we further compared the fracture micromorphology of the cured products of the two PN mixtures. In Fig. 12(b), it shows that the polymer cured with 4-APN shows a small number of small holes in a row, which are marked with red boxes. However, this phenomenon does not exist in the polymer cured with 1,3-DII. This shows that the catalyst 1,3-DII will not produce gas molecules during catalyzing the CN polymerization. This further proves the rationality of the mechanism
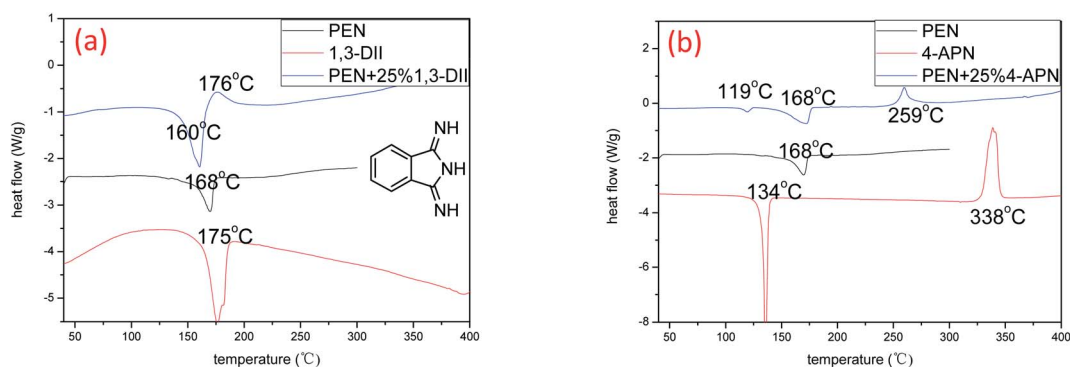

Fig. 11 DSC curves of PN resins with different catalysts ((a) the catalyst is 1,3-DII; (b) the catalyst is 4-APN).
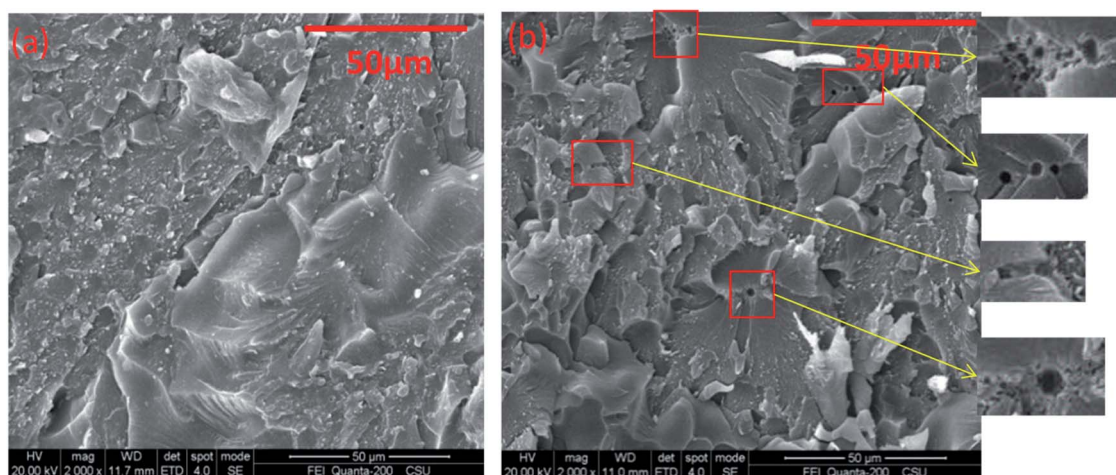
Fig. 12 Fracture profile of cured PN polymers with different catalysts ((a) the catalysts is 1,3-DII; (b) the catalysts is 4-APN).

proposed in this article. It is further shown that compounds containing ═NH are more suitable catalysts for PN resins.

4 Conclusions

In this article, 4-APN was taken as a representative of the widely used amino-type catalyst for PN resin and has been studied in detail. First, the trace gas released during the cure reaction was collected and detected by TG-IR-GC-MS. Compared with the standard spectrum, the gas was confirmed to be ammonia. Secondly, the curing reaction was tracked by online infrared. Combining with the results of TG-IR-GC-MS and online IR, the reaction mechanism of how ammonia was produced was proposed in this article for the first time. According to the reaction mechanism proposed in this article, a new strategy for selecting PN resin catalyst is proposed. Compounds containing ═NH are more suitable catalysts for PN resin than compounds containing –NH$_2$. As a result, the new catalyst 1,3-DII, selected according to the new strategy, not only has a good catalytic performance, but also can effectively reduce the voids generated by 4-APN polymerization. In addition, the heat release rate of curing reaction of the new catalyst is slower than 4-APN, and the curing temperature is lower, which is more advantageous for preparing thick-walled composite and reducing the preparation cost.

Conflicts of interest

There are no conflicts to declare.

Acknowledgements

Notes and references

1 B. Sun, Q. Lei, Y. Guo, H. Shi, J. Sun, K. Yang, H. Zhou, Y. Li, N. Hu, H. Wang and S. Fu, *Composites, Part B*, 2019, **166**, 681–687.
2 T. M. Keller, *Chem. Mater.*, 1994, **6**, 302–305.
3 X. Yang, K. Li, M. Xu and X. Liu, *Composites, Part B*, 2018, **155**, 425–430.
4 N. Mushtaq, G. Chen, L. R. Sidra, Y. Liu and X. Fang, *Polym. Chem.*, 2016, **7**, 7427–7435.
5 H. Wang, J. Wang, H. Guo, X. Chen, X. Yu, Y. Ma, P. Ji, K. Naito, Z. Zhang and Q. Zhang, *Polym. Chem.*, 2018, **9**, 976–983.
6 T. Butler, S. E. Alden, M. Taylor, S. Deese, D. A. Rider and M. Laskoski, *J. Polym. Sci., Part A: Polym. Chem.*, 2018, **56**, 2630–2640.
7 T. M. Keller, *Polymer*, 1993, **34**, 952–955.
8 Y. Huang, Y. Luo, M. Xu, Y. Lei and X. Liu, *Composites, Part B*, 2016, **106**, 294–299.
9 C. Yin, L. Sheng, Y. Yang, G. Liang, S. Xing, J. Zeng and J. Xiao, *RSC Adv.*, 2018, **8**, 38210–38218.
10 L. Sheng, J. Zeng, S. Xing, C. Yin, J. Yang, Y. Yang and J. Xiao, *High Perform. Polym.*, 2017, **29**, 13–25.
11 L. Sheng, C. Yin and J. Xiao, *RSC Adv.*, 2016, **6**, 22204–22212.
12 T. M. Keller and T. R. Price, *J. Macromol. Sci., Part A: Pure Appl. Chem.*, 1982, **6**, 931–937.
13 M. Wu, J. Xu, S. Bai, X. Chen, X. Yu, K. Naito, Z. Zhang and Q. Zhang, *Soft Matter*, 2020, **16**, 1888–1896.
14 Y. S. Tay, M. Liu, J. S. K. Lim, H. Chen and X. Hu, *Polym. Degrad. Stab.*, 2020, **172**, 1–7.
15 S. Bai, X. Sun, Z. Zhang, X. Chen, X. Yu and Q. Zhang, *ChemistrySelect*, 2020, **5**, 265–269.
16 H. Zhang, B. Wang, Y. Wang and H. Zhou, *Polymers*, 2020, **12**, 1–15.
17 Z. Weng, Y. Hu, Y. Qi, S. Zhang, C. Liu, J. Wang and X. Jian, *Polym. Adv. Technol.*, 2020, **31**, 233–239.
18 S. Bai, X. Sun, M. Wu, X. Shi, X. Chen, X. Yu and Q. Zhang, *Polym. Degrad. Stab.*, 2020, **177**, 1–10.

19 Y. Zu, F. Zhang, D. Chen, L. Zong, J. Wang and X. Jian, *Polymer*, 2020, **198**, 122490.

20 V. A. Bershtein, A. M. Fainleib, P. N. Yakushev, D. A. Kirilenko, K. G. Gusakova, D. A. Markina, O. G. Melnychuk and V. A. Ryzhov, *eXPRESS Polym. Lett.*, 2019, **13**, 656–672.

21 S. Ren, S. Zhang, W. Zhao, W. Wang, X. Miao and W. Song, *Polym. Adv. Technol.*, 2019, **30**, 1394–1402.

22 Y. Chen, A. Q. Dayo, H. Zhang, A. Wang, J. Wang, W. Liu, Y. Yang, Q. Qin and Y. Yang, *J. Appl. Polym. Sci.*, 2019, **136**, 1–10.

23 A. Medjahed, M. Derradji, A. Zegaoui, R. Wu and B. Li, *Mater. Sci. Technol.*, 2019, **35**, 661–668.

24 J. Ma, T. Liu, W. Wang and Y. Yang, *High Perform. Polym.*, 2019, **31**, 3–11.

25 A. Badshah, M. R. Kessler, Z. Heng, J. H. Zaidi, S. Hameed and A. Hasan, *Polym. Chem.*, 2013, **4**, 3617–3622.

26 G. Wang, Y. Guo, Z. Li, S. Xu, Y. Han, Z. Luo, L. Ye, H. Zhou and T. Zhao, *J. Appl. Polym. Sci.*, 2018, **135**, 1–8.

27 B. A. Bulgakov, K. S. Belsky, S. S. Nechausov, E. S. Afanaseva, A. V. Babkin, A. V. Kepman and V. V. Avdeev, *Mendeleev Commun.*, 2018, **28**, 44–46.

28 S. B. Sastri and T. M. Keller, *J. Polym. Sci., Part A: Polym. Chem.*, 1998, **36**, 1885–1890.

29 S. B. Sastri and T. M. Keller, *J. Polym. Sci., Part A: Polym. Chem.*, 1999, **37**, 2105–2111.

30 H. Sheng, X. Peng, H. Guo, X. Yu, K. Naito, X. Qu and Q. Zhang, *Thermochim. Acta*, 2014, **577**, 17–24.

31 Z. Chen, H. Guo, J. Yang, R. Zhao and X. Liu, *High Perform. Polym.*, 2013, **25**, 214–224.

32 B. Liang, J. Wang, J. Hu, C. Li, R. Li, Y. Liu, K. Zeng and G. Yang, *Polym. Degrad. Stab.*, 2019, **169**, 1–8.

33 W. J. Monzel, G. Lu, T. L. Pruyn, C. L. Houser and G. T. Yee, *High Perform. Polym.*, 2019, **31**, 935–947.

34 V. E. Terekhov, V. V. Aleshkevich, E. S. Afanaseva, S. S. Nechausov, A. V. Babkin, B. A. Bulgakov, A. V. Kepman and V. V. Avdeev, *React. Funct. Polym.*, 2019, **139**, 34–41.

35 Y. Zu, L. Zong, J. Wang and X. Jian, *Polymer*, 2019, **172**, 372–381.

36 G. Wang, Y. Han, Y. Guo, J. Sun, S. Wang, H. Zhou and T. Zhao, *Eur. Polym. J.*, 2019, **113**, 1–11.

37 Y. Liu, Z. Liu, W. Peng, Z. Lu, J. Hu, K. Zeng and G. Yang, *Polym. Int.*, 2019, **68**, 724–734.

38 Y. Han, D. Tang, G. Wang, Y. Guo, H. Zhou, W. Qiu and T. Zhao, *Eur. Polym. J.*, 2019, **111**, 104–113.

39 B. Sun, Q. Lei, Y. Guo, H. Shi, J. Sun, K. Yang, H. Zhou, Y. Li, N. Hu, H. Wang and S. Fu, *Composites, Part B*, 2019, **166**, 681–687.

40 J. Xu, H. Wang, Z. Zhang, K. Yang, P. Li, X. Chen, X. Yu, K. Naito and Q. Zhang, *J. Polym. Sci., Part A: Polym. Chem.*, 2019, **57**, 2287–2294.

41 H. Wang, Z. Zhang, P. Ji, X. Yu, K. Naito and Q. Zhang, *High Perform. Polym.*, 2019, **31**, 820–830.

42 Y. Liu, P. Ji, Z. Zhang, X. Yu, K. Naito and Q. Zhang, *High Perform. Polym.*, 2019, **31**, 1075–1084.